Experimental Thermal and Fluid Science 135 (2022) 110631

Contents lists available at ScienceDirect

Experimental Thermal and Fluid Science

journal homepage: www.elsevier.com/locate/etfs

An experimental approach to evaluate drying kinetics and foam formation in inks for inkjet printing of fuel-cell layers

Paolo E. Santangelo [a,b,*], Marcello Romagnoli [c,d], Marco Puglia [c]

[a] Dipartimento di Scienze e Metodi dell'Ingegneria, Università degli Studi di Modena e Reggio Emilia, Reggio Emilia, Italy
[b] Centro interdipartimentale per la ricerca En&Tech, Reggio Emilia, Italy
[c] Dipartimento di Ingegneria "Enzo Ferrari", Università degli Studi di Modena e Reggio Emilia, Modena, Italy
[d] Centro interdipartimentale per la ricerca InterMech – MO.RE., Modena, Italy

ARTICLE INFO

Keywords:
Liquid
Film
Evaporation
Solvent
Bubbles

ABSTRACT

Inkjet printing is a deposition technique that has remarkably evolved over the last two decades, becoming widely employed for various applications. Notably, it has proven very promising for catalyst and ionomer layer deposition in assembling CCM (Catalyst Coated Membranes) of PEMFC (Polymer Electrolyte Membrane Fuel Cells). However, fast drying of the processed inks at the outlet often causes nozzle clogging and foam formation within the supply circuit often yields poor release: these are the main challenges in applying inkjet printing on a large scale. So, an experimental approach for the evaluation of drying kinetics and foam formation in inks typically employed in fuel-cell manufacturing is presented. It allows to evaluate ink printability, compare different inks quantitatively and assess the performance of commonly used additives. Evaluation of drying kinetics is based on releasing ink droplets onto a support, then recording mass, ambient temperature and relative humidity. Foam formation is evaluated by filling a syringe with a known amount of ink, then injecting air at a set flow rate into the sampling volume: foam may be ultimately generated and its amount can be measured. Those relatively simple approaches were applied to various inks; validation was conducted by statistical analysis and by comparison with physical relationships and datasets available in the open literature.

1. Introduction

Fuel cells are electrochemical devices able to convert the chemical energy from an energy carrier – typically, but not exclusively, hydrogen – into electrical energy through redox reactions, with heat being produced as a secondary output of an exothermic process [1,2]: overall, the products of a fuel cell are heat and power, together with water, starting from a fuel and oxygen as reactants. Among the various types, Polymer Electrolyte Membrane Fuel Cells (PEMFC) are arguably the most promising, at least at low operative temperatures (below 100 °C), thanks to their robustness and durability [3]; they are currently employed in both stationary [4] and mobile applications [5]. The core of a PEMFC is the Membrane Electrode Assembly (MEA) that is where the electrochemical reactions take place [6]; it actually consists of the 2 electrodes – anode and cathode – and a solid membrane interposed between them. The main component of the electrodes is the catalyst (Platinum or Platinum/Ruthenium for Direct Methanol Fuel Cells), which is typically mixed with a perfluorosulphonic acid (PFSA) ionomer within carbon-supported nanoparticles [7]; the catalyst loading may differ between anode and cathode, with the former being typically lower than the latter [8]. Those materials are dispersed in liquid solvents to form a suspension, the actual ink that is used for deposition onto a solid substrate [9,10]. On the other hand, the PEMFC membranes consist of two components: a PFSA ionomer material, including -SO_3H groups that promote proton conductivity, and a reinforcement material, typically an expanded polytetrafluoroethylene (ePTFE) film providing mechanical strength. The ionomer is usually released as a dispersion within a liquid solvent, thus constituting an ink that is cast onto a substrate; the reinforcement material represents the inner layer of the membrane [11].

The conventional CCM (Catalyst Coated Membrane) manufacturing approach consists of the following sequential steps: depositing the catalyst inks onto decal-transfer carrier films; depositing the ionomer onto a carrier film, then onto the ePTFE film; removal of the membrane support film; hot pressing the catalyst layers against the membrane; final

* Corresponding author at: Dipartimento di Scienze e Metodi dell'Ingegneria, Università degli Studi di Modena e Reggio Emilia, Padiglione Morselli, Campus San Lazzaro, Via G. Amendola 2, 42122 Reggio Emilia, Italy.
E-mail address: paoloemilio.santangelo@unimore.it (P.E. Santangelo).

https://doi.org/10.1016/j.expthermflusci.2022.110631
Received 12 June 2021; Received in revised form 5 January 2022; Accepted 17 February 2022
Available online 19 February 2022

removal of decal-transfer carrier films [12,13]. However, as fuel cells are transitioning from low-volume to mass production [3], innovative manufacturing techniques [14,15], successfully employed in other sectors (e.g., ceramic tiles, electronics), have been explored to perform CCM roll-to-roll production, together with improving layer quality and reducing raw-materials consumption [16]. Notably, coating and printing techniques were recently employed to deposit the inks onto the substrate in a continuous process: ultrasonic spraying [17], gravure coating [18], knife and slot-die coating [19], screen printing [20] and inkjet printing [21]. Inkjet printing exhibits some advantages that seem to boost it at the forefront: as already determined for solar-cell manufacturing [22], its high resolution, capability of patterning at high speed and low associated waste of ink match the characteristics required by mass production. Unfortunately, fast evaporation of certain components of a multicomponent ink during both non-operating periods and normal functioning may result in accumulation of non-volatile materials at the nozzle outlet, thus generating a plug or a crust. This phenomenon, known as nozzle clogging [23], often implies printhead failure, which is hardly recoverable [24]. Among the various anti-clogging strategies (e.g., applying a shaking wave at the nozzle, inserting a vapor trap, using a recirculation system), adding humectants to the solvent allows reducing evaporation rate [25,26]; among the available chemicals, glycol compounds (e.g., ethylene glycol, polyethylene glycol, propylene glycol) appear the most suitable, as they are known not to poison the electrodes. Another issue that may affect inkjet printing performance is the presence of air bubbles within the ink, often due to air entrainment while the supply circuit is being filled or through the nozzle outlet during non-operating periods. This phenomenon may yield foam formation, thus ultimately causing poor, inhomogeneous or even failed ink deposition [27]. A common and largely employed solution to avoid or reduce foaming consists of adding defoamers (e.g., non-ionic, silicone-based) to the ink, which fosters breakdown in bubbles [24].

Determining whether an ink may undergo fast drying and whether it may be prone to foam formation is rather significant for assessing its inkjet printability, especially by industrial printers that host large amounts of ink within the supply circuit. Moreover, the quantitative comparison between different inks – either endowed with additives or not – in terms of drying kinetics and foam formation is also instrumental. The present work is aimed at providing a relatively simple, yet quantitatively sound experimental approach to the purpose. As for ink drying onto a solid surface, it is worth recalling the combined three-fold methodology (infrared thermography, X-ray radiography, computed tomography) by Fournier et al. [28], applied to typical PEMFC substrates; however, their study is mostly focused on liquid/solid interaction, with a detailed analysis of the drying behavior through the liquid film. The seminal study by Can [29], also conducted by infrared thermography, allowed highlighting the constant-rate drying period even by a transport model; subsequent works were then focused more on the conditions that facilitate the drying process through convective heat transfer [30,31]. A strong foundation for the approach developed here to evaluate drying kinetics is embodied by the method proposed by Ward et al. [32]: a simple quality control tool was devised, with evaporation rate being the parameter that allows identifying compliance with ink specifications. A formulation for predicting evaporation rate developed by Ward et al. [32] was also challenged against the results from the present work. As for the evaluation of foam formation, a simple and fairly robust method was developed, with the early work by Brady and Ross [33] standing as a prominent reference, even though their experimental apparatus was based on injecting pure nitrogen into the tested liquid, while keeping the vessel at constant, high temperature, so that bubbles were made rapidly rise vertically. Interesting studies have also been conducted for decades on foam formation in organic compounds related to food industry [34,35] and on foam generation and transport in pipes, both horizontal [36] and vertical [37]. However, the involved mechanisms are slightly different from those considered in the present research, either as they stem from biological processes (e.g., fermentation) or because the scale is significantly larger. As more recent sources of inspiration, the works by Nishioka and Ross [38] and Lunkenheimer and Malysa [39] show simple setups, where bubbles are generated within the tested liquid by air injection. However, the here presented apparatus was developed to resemble the operating conditions of an industrial inkjet printer, so air was supplied within the inks at a constant flow rate, rather than injecting discrete air bubbles.

2. Materials and methods

2.1. Drying kinetics

The developed apparatus consists of a PTFE cylindrical support (50 mm diameter, 15 mm height) with a machined blind cylindrical hollow – the dimensions of which (15.9 mm diameter and 0.7 mm depth) were set to allow hosting a slight excess of the amount of ink released in each test (i.e., 0.1 ml), a 1 ml syringe, an analytical balance equipped with an enclosure (*SBC 32* model by *SCALTEC Instruments*, ±0.1 mg accuracy), a camera (*MHS-PM5* model by *Sony*, resolution: 1280 × 720 pixel, acquisition rate: 30 frames per second) and a Wi-Fi temperature and relative humidity (RH) data-logging sensor (by *Lascar Electronics*, accuracy: ±0.3 °C for temperature readings and ±1% for relative humidity). A sketch (Fig. 1) and a photo (Fig. 2) of the whole setup are presented: the balance hosts the PTFE support onto its measuring plate. It is worth noting that PTFE was employed as the solid substrate because of its relatively easy machinability and not with relation to PEMFC membranes: in fact, clogging in industrial inkjet printer occurs on surfaces that can be made of glass, plastic or metal, depending on the selected printhead, internal framework and reservoir.

A promising strategy to prevent inks from drying and leaving solid deposits that ultimately result in clogging consists of coating the nozzle plate with non-wetting layers [40]. However, the repelling effect of those layers should be verified against each released ink. The PTFE substrate selected for the present experiments can be regarded as conservative, since high wettability (i.e., contact angle lower than 90°) was proved for each tested ink, thus implying that clogging may actually occur throughout the drying process. The devised apparatus mostly aims at evaluating evaporation of the liquid phase (i.e., the solvent) and comparing inks: the developed PTFE support is capable of ensuring the same area of the ink exposed to ambient air and available for convective heat transfer over the entire set of performed tests, as well as guaranteeing that the same surface of the ink be in direct contact with a solid body and available for thermal conduction. So, consistency between the various conducted experiments applied in that regard. Moreover, a hollow-shaped cavity allows imposing a uniform radial extent to the deposited amount of ink, even though its height-to-diameter ratio (i.e., an expression of its aspect ratio) is remarkably small. The overall approach to evaluate drying kinetics is founded on acquiring the mass trend through the drying process for all the tested inks, so that a comparison between them can then be directly obtained.

The drying kinetics of five inks was tested; even though the formulation is proprietary (by *Johnson Matthey Fuel Cells*), the selected inks are representative of those typically employed to deposit the anode and the cathode layers (PEMFC electrodes) and the ionomer layer of the PEMFC membrane. Notably, Cathode is representative of a cathode ink, with a mixture of deionized water and a low-boiling-point (<100 °C) alcohol employed as the solvent; Anode 1 is representative of an aqueous anode ink; Anode 2 is representative of an anode ink, with a mixture of deionized water and the same alcohol as in Cathode employed as the solvent; Ionomer is an ionomer solution, with a mixture of deionized water and another low-boiling-point alcohol employed as the solvent. The solid content and the solvent of each tested ink are reported and summarized in Table 1. A mixture of Cathode and ethylene glycol (about 10 wt% of the mixture) was also tested, as that humectant was selected among those commonly used to reduce evaporation rate and acceptable for fuel-cell applications (Section 1).

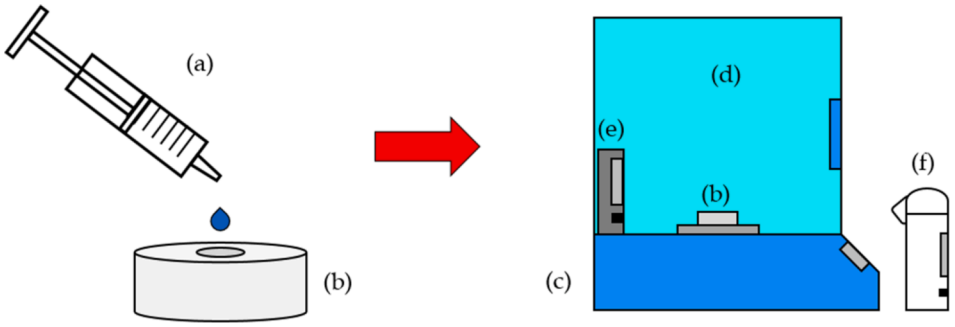

Fig. 1. Sketch of the experimental apparatus to evaluate drying kinetics: (a) syringe, (b) support, (c) analytical balance, (d) enclosure, (e) temperature and relative humidity sensor, (f) camera.

Fig. 2. Photo of the experimental apparatus to evaluate drying kinetics.

Table 1
Solid content and solvent employed in each tested ink.

Ink	Solid content (wt%)	Employed solvent
Cathode	10–20	deionized water/alcohol
Anode 1	20–30	aqueous
Anode 2	5–15	deionized water/alcohol
Ionomer	5–15	deionized water/alcohol

As mentioned in the Introduction (Section 1), platinum concentration is higher for the Cathode ink. Every ink was stirred – manually at the beginning, then by ultrasonic and magnetic stirring – for a few hours prior to starting actual tests to avoid inhomogeneous distribution of the components, since jellification of the solid content is known to occur in fuel-cell inks. Since strict requirements are imposed to inks in terms of viscosity (generally lower than 30 mPa s [23]) for being considered inkjet-printable, viscosity of the tested inks was also measured by an optical rheometer (*Fluidicam RHEO* by *Formulaction*, featuring and accuracy of ±1%), capable of applying shear rate values even in the order of some thousands of s^{-1}, thus including the high shear-rate operating region. Measurements were conducted at 25 °C. The results are shown in Fig. 3 for three inks representative of the layers to be deposited (i.e., Cathode, Anode 2 and Ionomer): viscosity appears overall rather constant over the 1000–15,000 s^{-1} range of shear rate and consistently lower than 30 mPa s, with the average percentage deviation from the mean value being lower than 30% for Anode 2 and lower than 3% for Cathode and Ionomer, and average standard deviation being lower than

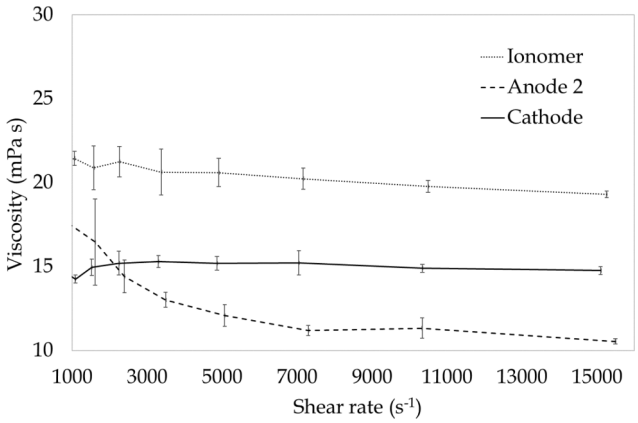

Fig. 3. Viscosity profiles of three representative inks (Anode 2, Cathode and Ionomer) over the 1000–15,000 s^{-1} shear-rate span.

1 mPa s, which generally hints at a Newtonian behavior of the employed inks over most of the tested range of imposed shear rate and demonstrates they comply with the previously mentioned requirement.

The experimental procedure to achieve a quantitative evaluation of ink mass-loss trend started with weighing the PTFE support to offset its tare weight throughout the measurements. About 0.1 ml of ink was then gently deposited onto the PTFE support, filling the already described hollow (Fig. 4); that value of the released ink volume was identified as the smallest amount significant with respect to the accuracy of the employed analytical balance. The ink drying process was videorecorded, with its mass readings being acquired every 30 s for 45 min, also monitoring ambient temperature and relative humidity to verify consistency between all the performed tests in terms of environmental conditions.

Acquisition frequency was set at the reported value after some preliminary tests proved any higher frequency poorly significant for better capturing the evaporation mechanism. It is worth clarifying that the ink was exposed to quiescent ambient air: the sampling region was enclosed within the case of the balance; however, the volume of the enclosure was sufficiently larger than the ink volume to avoid potential saturation, an unlikely event *per se*. Ambient temperature and relative humidity were rather constant and equal to 18 ± 2 °C and 45% ± 6% respectively within the enclosure throughout the whole experimental campaign. The procedure was repeated five times for each tested ink to assess statistical variability, repeatability and ultimately experimental uncertainty; notably, the average trend over the five repeated tests was calculated for each ink, then also calculating standard deviation at each acquisition [41]. As repeatability of the experiments was deemed overall high, five repeats appeared sufficient to build a representative dataset. After that, a small amount of the same tested ink (a few milliliters) was deposited on a watch glass and let dry for 24 h to obtain an experimental

Fig. 4. Ink deposition onto the PTFE support, within the hollow.

evaluation of solid and liquid concentration, which served as an assessment against the values of solid and liquid concentration provided by the ink producer, with the two proving consistent with each other. This operation was applied to each tested ink, including the one endowed with ethylene glycol. As a preliminary assessment of the ability of the proposed methodology to capture the involved physics, a test was also conducted on pure ethylene glycol, a well-known hygroscopic substance. As expected, after 24 h of exposure in the hollow, its mass had actually increased by about 14.8%, since water absorption from the environment was predominant over evaporation.

The mass loss trend was initially analyzed under the form of m_i/m_0 ratio, where m is mass, i refers to the generic ith acquisition and 0 refers to the initial acquisition upon deposition. However, since solid and the liquid fraction of each ink is known, it was also possible to calculate mass loss trend as referred to the sole liquid fraction (i.e., the part of the ink available for evaporation):

$$\frac{m_{l,i}}{m_{l,0}} = \frac{m_i - m_{s,0}}{m_0 - m_{s,0}}, \tag{1}$$

where l refers to the liquid phase, s refers to the solid phase and $m_{s,0}$ can be calculated as:

$$m_{s,0} = m_0(1 - x). \tag{2}$$

The liquid fraction x is defined as:

$$x = \frac{m_{l,0}}{m_0}. \tag{3}$$

Furthermore, mass loss rate – the actual evaporation rate – was also quantitatively evaluated as the derivative of mass with respect to time. Notably, the derivative was calculated under the approximation of any involved differential quantity to a finite difference. Evaporation rate is presented here in non-dimensional form, with the initial mass of the liquid fraction employed to nondimensionalize mass and the sampling period employed to nondimensionalize time: it embodies a ratio to the constant evaporation rate that would yield full drying throughout the sampling period. For the generic ith acquisition, mass loss rate is expressed as:

$$\dot{m}^*_{evap} = \frac{dm^*}{dt^*} \cong \frac{\Delta m^*}{\Delta t^*} = \frac{(m_{i-1} - m_{i+1})(t_f - t_0)}{(t_{i+1} - t_{i-1})m_{l,0}}, \tag{4}$$

where * refers to dimensionless quantities, *evap* stands for evaporated, t is time and f refers to the final acquisition. For the first acquisition ($i = 0$) the following expression was employed:

$$\dot{m}^*_{evap} = \frac{dm^*}{dt^*} \cong \frac{\Delta m^*}{\Delta t^*} = \frac{(m_0 - m_1)(t_f - t_0)}{(t_1 - t_0).m_{l,0}}, \tag{5}$$

whereas for the final acquisition ($i = f$) the following expression was employed:

$$\dot{m}^*_{evap} = \frac{dm^*}{dt^*} \cong \frac{\Delta m^*}{\Delta t^*} = \frac{(m_{f-1} - m_f)(t_f - t_0)}{(t_f - t_{f-1})m_{l,0}}. \tag{6}$$

Data points are sufficiently scattered over the sampling period thanks to the selected acquisition frequency, so no moving average over a subset of data larger than that employed in Eq. (4) for each acquisition was deemed necessary, since the trends calculated for each tested ink resulted as relatively smooth.

As a comparison with existing predictive formulations, the measured mass loss trend was compared with the evaporation rate obtained through the diffusive model proposed by Ward et al. [32], which relies on the Cottrell equation [42] that expresses the analogy between evaporated mass and current flow in electrochemistry (*diffusive model* thereafter). Notably, the contribution by Cottrell [42] and Buck et al. [43] consists of relating current intensity with time in an electrochemical system operating at controlled potential, while Ward et al. [32] applied a principle of similarity between evaporation rate and electrochemical systems: weighted stoichiometric molar charge is taken as the equivalent to molar mass of the evaporating solvent. The physicochemical properties of the tested inks are considered as known parameters. The underlying theory is embodied by Fick's laws [44–46]: the first Fick's law describes mass diffusion in a binary mixture as $J = -CD.\nabla\phi$, where J is diffusive molar flux, D is the binary diffusion coefficient, C is molar concentration and ϕ is molar fraction of the generic species; the second Fick's law expresses diffusion in transient conditions and by one-dimensional analysis as $\frac{\partial C}{\partial t} = -D\frac{\partial^2 C}{\partial y^2}$, where y is the coordinate perpendicular to a generic surface. Ward and Tordai [47] combined those formulations to obtain the diffusion rate per unit area across a generic surface at $y = 0$:

$$\left(\frac{\partial m}{\partial t}\right)_{y=0} = -\frac{DC}{\sqrt{\pi Dt}} \tag{7}$$

So, in the present work the measured mass loss trends were compared with the values calculated through a model based on the following equation proposed by Ward et al. [32] to predict evaporation rate in their experimental configuration, which stems from Eq. (7):

$$\frac{dm}{dt} = -MS\frac{xp}{RT}\frac{D}{\sqrt{\pi Dt}}, \tag{8}$$

where M is the molar mass of the solvent(s), p is the solvent vapor pressure, R is the molar gas constant (8.3145 J mol^{-1} K^{-1}), T is the absolute temperature, D is the diffusion coefficient of the solvent(s) (vapor) and S is the surface area of the exposed interface ($S = \pi d^2/4$,

with d being the diameter of the hollow). It is worth noting that the term $M\frac{xp}{RT}$ corresponds to molar concentration C of Eq. (7), referred to the solvent in the gaseous state. In case of inks including more than one solvent in their formulation (i.e., multicomponent liquid phase), M, p and D of the liquid mixture were calculated as the weighted average, with mass concentration of each solvent being the weighting factor. Integrating Eq. (8) from an initial limit at $t_0 = 0$ to a generic time t [32,47], with $m = m_0$ at $t_0 = 0$, mass loss (i.e., the amount of evaporated solvent) can be obtained as:

$$m - m_0 = -2MS\frac{xp}{RT}\sqrt{\frac{Dt}{\pi}}. \tag{9}$$

The formulation expressed by Eq. (9) reflects the one developed by Langmuir and Schaefer [48] to model ion diffusion into monolayers.

The comparison between different inks can be generally performed through Eq. (9), ultimately normalized by dividing both members by m_0:

$$\frac{m}{m_0} = 1 - 2\frac{M}{m_0}S\frac{xp}{RT}\sqrt{\frac{Dt}{\pi}}. \tag{10}$$

As opposed to the study by Ward et al. [32], where a modified Stefan-Winklemann tube was employed and the solvent supply could be considered infinite, in the present work the ratio between area exposed to ambient air and total ink volume is high and the solvent mass loss over time is not negligible compared to the initial mass available for evaporation (i.e., the initial liquid fraction). So, the amount of solvent was considered variable over time and recalculated at each ith acquisition as:

$$x_i = \frac{\left[x_0 - \left(1 - \frac{m_{i-1}}{m_0}\right)\right]}{\frac{m_{i-1}}{m_0}}. \tag{11}$$

Moreover, another variation was introduced in the calculations with respect to the diffusive model embodied by Eq. (9): the time interval considered for each integration was 30 s, a timespan that corresponds to the interval between two consecutive acquisitions through mass recording in each experiment. In the generic interval $[t_{i-1},t_i]$, the amount of solvent available for evaporation was considered constant. Assuming this *Ansatz*, mass m in Eq. (9) turns into m_i and m_o in Eq. (9) turns into m_{i-1}, which yielded to express the diffusive equation referred to the generic interval:

$$m_i = m_{i-1} - 2MS\frac{x_i p}{RT}\sqrt{\frac{D(t_i - t_{i-1})}{\pi}}. \tag{12}$$

So, the whole evaporation process was subdivided over a set of intervals, each of which featuring a 30 s timespan; Eq. (12) was then applied to every interval, thus making the model practically independent of the condition of infinite solvent supply. In a similar manner to Eq. (10), the comparison of the diffusive model with the experimental dataset was performed through a normalized expression:

$$\frac{m_i}{m_0} = \frac{m_{i-1}}{m_0} - 2\frac{M}{m_0}S\frac{x_i p}{RT}\sqrt{\frac{D(t_i - t_{i-1})}{\pi}}. \tag{13}$$

As another term of comparison, the diffusive model developed by Saito [49] for the isotropic diffusion case as time approaches infinity provides a formulation for the limiting evaporation rate:

$$\frac{dm}{dt} = -2MDd\frac{xp}{RT}. \tag{14}$$

Under the simplifying assumption $dm/dt \approx \Delta m/\Delta t$ and acknowledging that $\Delta m_i = m_i - m_0$ and $\Delta t_i = t_i - t_0$, mass loss could also be evaluated by applying evaporation rate at constant isotropic diffusion to the whole evaporation process from deposition through a generic time t_i:

$$\frac{m_i}{m_0} = 1 - 2\frac{M}{m_0}Dd\frac{xp}{RT}t_i, \tag{15}$$

where $t_0 = 0$ as in Eq. (9). This additional model is inherently approximate, since it relies on a limiting constant value of evaporation rate employed over the entire transient process, yet it allowed assessing to what extent the tested inks can be considered isotropic in terms of diffusion.

The involved physicochemical properties of the solvents included in the tested inks are reported in Table 2. It is worth clarifying that the listed values of diffusion coefficient refer to diffusivity of the vapor in a binary mixture with dry air.

2.2. Foam formation

As reviewed in the Introduction (Section 1), the developed methodology is aimed at assessing quantitatively foam formation in inks and stands as a variation of the rising bubble technique, even recently employed to investigate the moving gas-liquid interfaces [57]. In this approach, a single gas bubble is formed at the bottom of a liquid column and rises as a result of buoyancy, while its motion is followed by photographic techniques. However, the main focus is here on determining the extent to which an ink is prone to foam formation as air is entrained within, rather than studying how a single air bubble moves through; so, the devised apparatus is based on injecting a certain volume of air into quiescent ink. This air flow rate can be measured and was kept consistent through the test series to perform a comparison between different inks. As comparing the different inks is the ultimate scope, the injected flow rate was merely set as the value that allowed avoiding overflow of the ink container for the case exhibiting the higher foam formation.

Notably, the here presented setup consists of a 15 ml graduated test tube made of polypropylene, filled with a defined amount of ink. A straight and thin tube is then placed inside the graduated tube, ensuring that its outlet lightly touches the bottom of the graduated tube. The thin tube is connected to a 100 ml syringe by flexible piping. The syringe operates *de facto* as a volumetric pump: pushing the plunger of the syringe leads to inject air into the ink through the hydraulic circuit that ends with the thin tube, thus potentially generating the bubbles. In order to guarantee constant air supply over all the performed tests, the plunger is pushed by a linear actuator controlled via an Arduino board. The nominal air flow rate is 1.25 ml s^{-1} (10 ml discharge over 8 s). The experimental apparatus is shown in the photo of Fig. 5 and in the sketch of Fig. 6.

As the actual measurement, immediately after the air supply stops, the volume of the generated foam is measured and recorded. The differential volume within the graduated tube serves as an indicator of the tendency of an ink to generate foam and it was calculated as:

$$\Delta V = V - V_u, \tag{16}$$

where V is the volume read on the graduated scale and u refers to the initial undisturbed volume ($V_u = 2.75$ ml, thin tube immersed volume included). This approach to evaluate foam formation can also be employed to assess how persistent the generated foam is over time, which is a quantitative index of foam stability [58]: readings of foam height on the graduated scale can be made at various times once air injection stops. An empirical description of foam evolution over time is provided by the formulation proposed by Ross [59]:

Table 2
Physical properties of the various solvents.

Property	Substance		
	Water	Alcohols[1]	Ethylene glycol
M (kg mol^{-1})	0.01802 [50]	<0.1 [53]	0.06207 [55]
p at 20 °C (Pa)	2300 [51]	~ 10^3 [53]	6.5 [56]
D at 25 °C (m^2 s^{-1})	2.6 × 10^{-5} [52]	~ 10^{-5} [54]	10.05 × 10^{-6} [54]

[1] Since ink formulation is confidential (Sub-section 2.1), the data for the involved alcohols are reported here only as orders of magnitude; reference is also provided to the generic database and not to the specific chemical compounds.

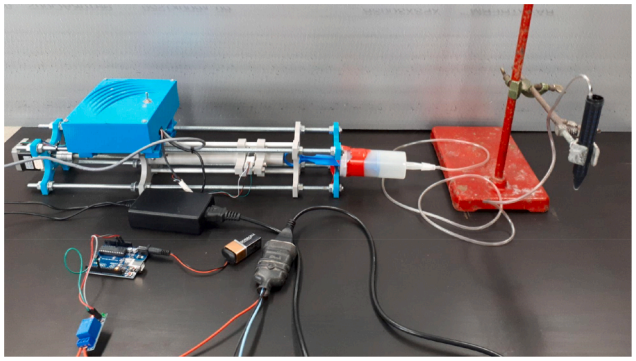

Fig. 5. Photo of the experimental apparatus to evaluate foam formation.

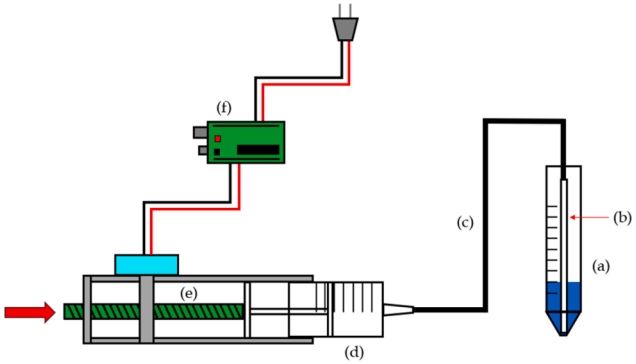

Fig. 6. Sketch of the experimental apparatus to evaluate foam formation: (a) graduated test tube, (b) thin tube, (c) flexible piping, (d) syringe, (e) linear actuator, (f) Arduino board.

$$\frac{\Delta V}{\Delta V_0} = e^{-\alpha t}, \tag{17}$$

where ΔV is the foam volume corresponding to a reading made at a generic time t, 0 is the initial reading (i.e., foam volume read immediately after air injection is stopped, which corresponds to $t = 0$) and α is a constant dependent on temperature and on the nature of the liquid from which the foam is formed [59]. The formulation by Ross [59] was employed in the present study to assess how the proposed measurement method is able to quantitatively evaluate foam stability.

However, reading foam height in the graduated tube over time is feasible only for transparent or semitransparent inks, since the trace left by an opaque ink onto the tube walls while foam is in the growing phase hardly allows to visually identify its reduction once air injection is over, as depicted in the photos of Fig. 7, where the graduated tube is shown before and after air injection. Therefore, foam formation in inks containing carbon-supported particles – almost all the catalytic inks – could be evaluated only in terms of maximum differential volume. On the other hand, foam stability and comparison with the theoretical formulation of Eq. (17) could be performed for ionomer inks. It is also worth remarking that wettability of the inks against the walls of the graduated tube may affect the height reached by the foam within the tube. In the present work, the polypropylene surface proved wettable by all the tested inks (i.e., contact angle lower than 90°), so a comparison could be made among them under consistent conditions. However, comparison between inks including chemicals – mainly solvents – particularly different from those involved in the present study may be performed once and if their wettability is determined as consistent. In a similar manner, the same preliminary assessment may be conducted if the selected graduated tube is made of a different material (likely a different polymer).

The proposed methodology is somewhat similar to the one developed

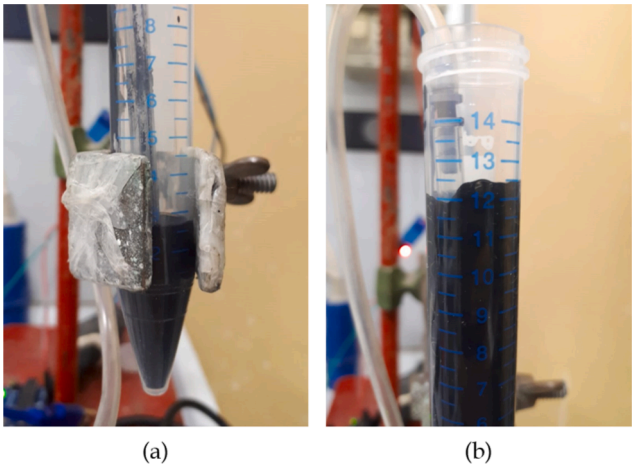

Fig. 7. Graduated test tube before (a) and after (b) air injection.

by Lunkenheimer and Malysa [39]; however, in the present work air is not supplied manually, but through a controlled actuator to ensure high – virtually flawless – repeatability. Moreover, the air flow rate is not released from the bottom, but it comes from a tube that slightly touches the bottom of the graduated tube, thus simplifying the whole apparatus: there is no need for an *ad hoc* glass column and a three-way valve to stop the air supply.

As for every pure ink mentioned in Sub-section 2.1 with regard to drying kinetics (Cathode, Anode 1, Anode 2 and Ionomer), the procedure was repeated five times to assess the repeatability and experimental uncertainty, which are expressed in terms of average values and standard deviation [41]. As mentioned in Sub-section 2.1, repeatability of the experiments was deemed sufficiently high to consider five repeats a representative dataset. Furthermore, two non-ionic (S1 and S3) and one silicone-based (S2) surfactants were tested as additives to one of the inks (Anode 2) – a choice made for the sake of consistency – under a concentration of 1 wt%, suggested by the producer. In inkjet printing, surfactants are often used for wetting enhancement [60]: if the surface tension of the solvent mixture is high, a surfactant may be included in the formulation to reduce it, which promotes ink absorption rate onto the substrate [60]. In some cases, surfactants are also used as defoamers, mainly coupled with aqueous solvents [60]. However lower dynamic surface tension often implies higher tendency to generate foam, yet also shorter bubble lifetime [61]; therefore, a method allowing to quantify advantages and disadvantages brought by a surfactant used as a defoamer can be quite significant.

3. Results

3.1. Drying kinetics

The mass loss trend evaluated through the experiments is presented in Figs. 8 and 9, which show how the evaporation of the liquid fraction (i.e., the solvent, Table 1) evolves over time with reference to the whole initial mass and to the liquid initial mass, respectively. The curves appear physically sound: the experimental setup (Sub-section 2.1, Fig. 1) yields a liquid film that even initially features a rather flat meniscus, with the mass loss trends resembling qualitatively those of droplets (spherical caps) gently released onto a solid surface with a small contact angle (initial angle $\leq 15°$, [62]). Notably, the profiles exhibit an initial steeper decrease that lasts about 600 s, then followed by a decay under a milder slope, arguably as a result of the inherent flattening of the meniscus through evaporation, which implies a reduction of the surface exposed to quiescent air and so to convective heat transfer. Those observations are strengthened by mass loss rate trend presented in Fig. 10. Regardless of the cusps typical of approximating derivatives by finite

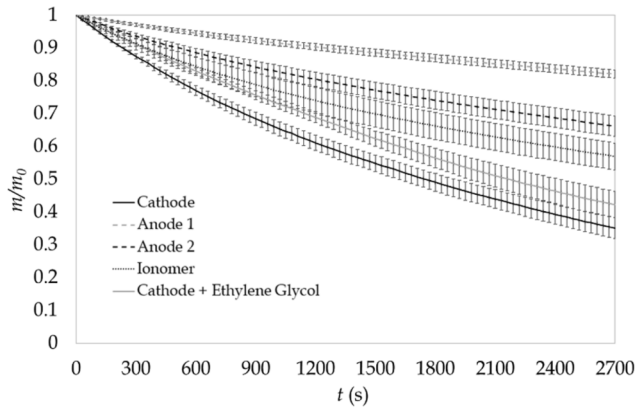

Fig. 8. Mass loss trend (referred to initial mass) through evaporation.

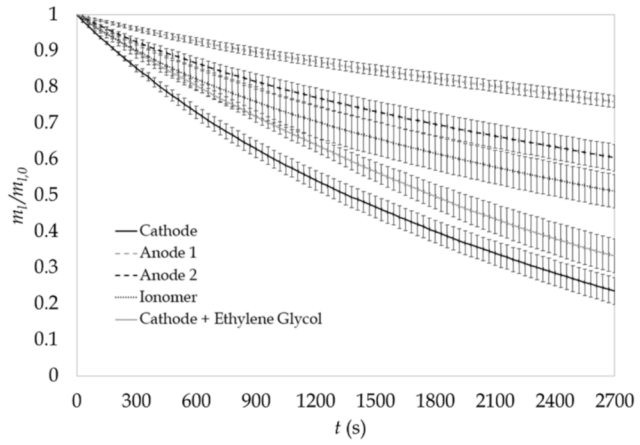

Fig. 9. Mass loss trend (referred to initial liquid mass) through evaporation.

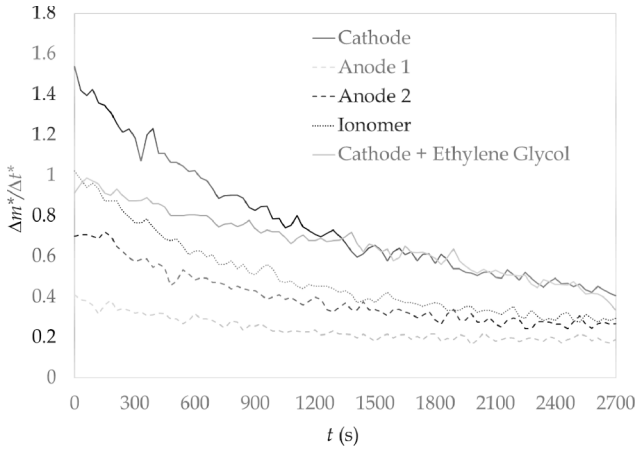

Fig. 10. Non-dimensional mass loss rate trend as evaluated by Eqs. (4)-(6).

differences, the ranking among different inks is consistent with that from mass loss evaluation (Figs. 8 and 9) and allows supporting the proposed methodology.

For instance, it is possible to observe that the effect of ethylene glycol used as an additive to reduce the evaporation process is effective especially at the beginning of the exposure to ambient air. Cathode initially evaporates under a non-dimensional rate bigger than 1, which is due to the involved solvent and, if kept constant, would yield full drying prior to the end of the sampling period. On the other hand, the presence of ethylene glycol mixed with Cathode implies a sharp reduction in initial evaporation rate, whereas the two trends tend to collapse onto each other from about 900 s through to the end, with an almost full overlap occurring from about 1300 s. Since ethylene glycol is a virtually non-evaporating liquid, its inclusion results in a lower fraction prone to evaporation at the beginning, which explains the large difference between the two trends over the first 900 s in both Figs. 9 and 10; an almost constant difference then follows from about 900 s, as evaporation of the volatile components is largely completed.

Volatility is clearly the most significant factor in explaining the different trends. It is apparent that the inks containing alcohol as a solvent (Cathode, Anode 2, Ionomer) exhibit a higher tendency to evaporate, thus featuring a generally bigger evaporation rate (i.e., mass loss rate, Fig. 10): both the involved alcohols are more volatile than pure water, while the one included in the Ionomer is also more volatile than the one included in Cathode and Anode 2 [63], which supports the observed trends. The mass loss trends shown for pure solvents [32] also appear to substantiate the aforementioned explanation for the different evaporation rates found by the here proposed methodology. The relationship between mass loss rate and solid content is less straightforward, even though the cathode inks appear to evaporate at a faster rate, which can be connected to the higher platinum content. However, the chemical bonds that may hold between the involved liquid and the solid species may affect the evaporation process, yet they exceed the scopes of the present work, also currently being not fully known or understood. A relationship between drying kinetics and viscosity may also hold, mostly as a result of the latter being ultimately an expression of how molecules interact [64]. However, the presented approach is not aimed at highlighting that physical connection, nor was it apparent from the conducted experiments, given the rather similar profiles and values exhibited by the tested inks in terms of viscosity (Fig. 3).

As shown in the curves of Figs. 8 and 9, standard deviation is quite low over the whole dataset for each tested ink; the maximum value found through statistical analysis is ± 0.05, occurred for Ionomer, which appears to support repeatability of the conducted experiments, thus ultimately emphasizing the robustness of the proposed experimental approach. No standard deviation is presented for mass loss rate, because curves of different inks overlapping may result in difficult identification of the error bars. However, average standard deviation calculated for mass loss rate is in the order of 10%, which also hints at the substantial repeatability of the proposed approach.

Fig. 11 shows the mass loss trends calculated through the diffusive model described in Sub-section 2.1 and consisting of Eq. (13) applied to each 30 s interval. Comparing the profiles of the same inks between experimental (Fig. 8) and predicted datasets (Fig. 11), it appears both experiments and model show the same ranking between inks in terms of evaporation rate, even including the ink endowed with ethylene glycol; this finding supports the proposed approach, given the generic

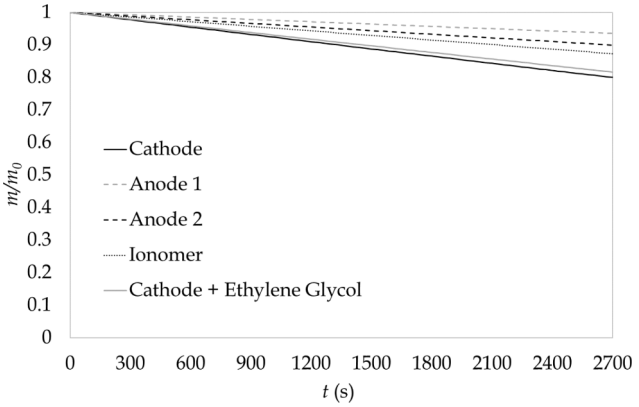

Fig. 11. Mass loss trend calculated through the diffusive model.

applicability of the diffusive model to predict evaporation rate [32]. However, quantitative discrepancies can be observed between predicted and experimental trends, which result in the diffusive model generally underestimating the evaporation rate.

On the other hand, Fig. 12 shows the mass loss trend calculated by Eq. (15), which is based on the approximation of evaporation rate equal to that occurring as time approaches infinity (i.e., limiting evaporation rate) and infinite solvent supply [49]. This would imply the highest evaporation rate possible in the case of isotropic diffusion.

Mass loss rate and consequently mass loss are obviously higher as the limiting rate applies (Fig. 12), when compared to those yielded by the diffusive model (Fig. 11); however, even if the limiting evaporation rate is employed through the whole process – an inherent approximation – the ranking among different inks is consistent with both the experimental dataset and that predicted by the diffusive model. Figs. 13-17 present the comparison between experimental results and the trends yielded by the two models (i.e., the diffusive model and that based on limiting evaporation rate) for each tested ink.

All the inks exhibit a steeper slope in the experimental mass-loss trend, compared to that featuring both the predicted, in the initial phase (i.e., the timespan that ranges from deposition through the 600–1200 s mark). That translates into a maximum percentage underestimation of the mass loss by the diffusive model in a range from less than 12% (Anode 1) to less than 45% (Cathode). This behavior can be explained as both the predictive models are founded on the isotropic diffusion phenomenon. However, mass-transport mechanisms at the gas/liquid interface can be remarkably affected by anisotropic diffusion, which implies the diffusion coefficient varies from axial to radial direction [32]. Notably, Ward et al. [32] observed that several inks exhibit an anisotropic behavior; assuming the diffusion coefficient from the available open literature as the radial one, they found that the axial diffusion coefficient could be larger even by a factor of eight, depending on the employed solvent. The longstanding quest for quantitative assessment of the diffusion coefficient in anisotropic substances falls beyond the scopes of the present work. However, it can be observed that some inks exhibit an experimental mass-loss trend that tends to fall between the one predicted by the diffusive model and that predicted under the limiting evaporation rate within the sampling time (i.e., the anode inks; Figs. 16 and 17), whereas others exhibit larger mass loss over the whole sampling time (i.e., the cathode inks; Figs. 13 and 14). So, the former seem more isotropic than the latter in terms of diffusion, even though the slope of all the experimental trends (i.e., the evaporation rate) tends to become asymptotically smaller than the limiting value (Figs. 13-17), as expected.

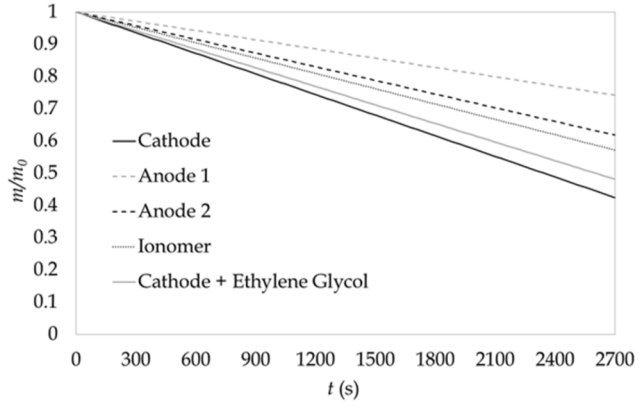

Fig. 12. Mass loss trend calculated as limiting mass loss rate is applied to the whole evaporation process.

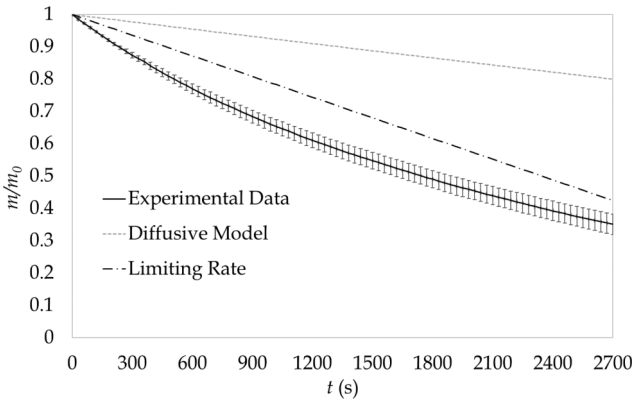

Fig. 13. Mass loss trends for Cathode ink (experimental and predicted).

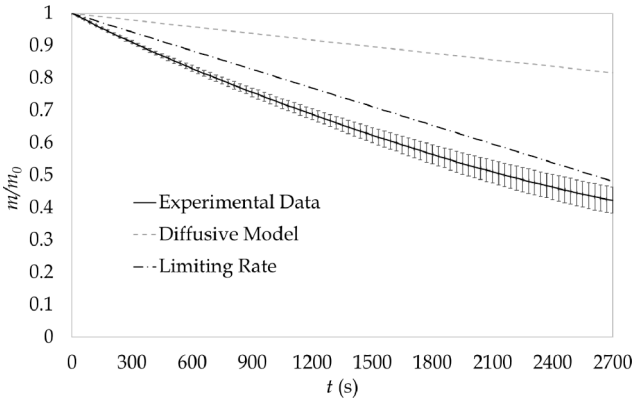

Fig. 14. Mass loss trends for Cathode and Ethylene Glycol ink (experimental and predicted).

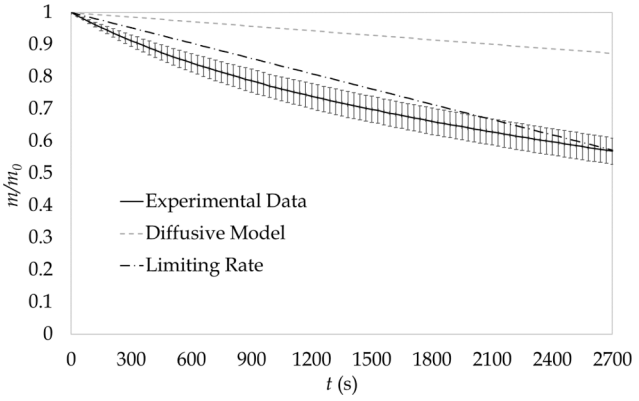

Fig. 15. Mass loss trends for Ionomer ink (experimental and predicted).

3.2. Foam formation

The amount of foam generated immediately after air injection into the tube is stopped (Sub-section 2.2) is presented in Fig. 18 as ΔV_0, where *0* refers to the reading on the graduated scale immediately after shutdown of air supply. Most inks exhibit a rather low standard deviation (in the order of ±0.5 ml), which supports the repeatability of the experiments, thus also making the approach quite robust. However, there is evidence of bigger standard deviation for Anode 2 endowed with surfactant S2 (±1.2 ml); that could be also related to the dual action performed by the selected surfactants [60,61]: bubble formation may even be emphasized by the lower surface tension, yet they may have a

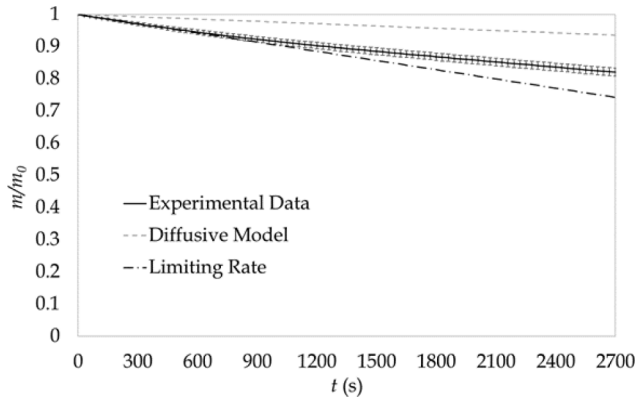

Fig. 16. Mass loss trends for Anode ink (experimental and predicted).

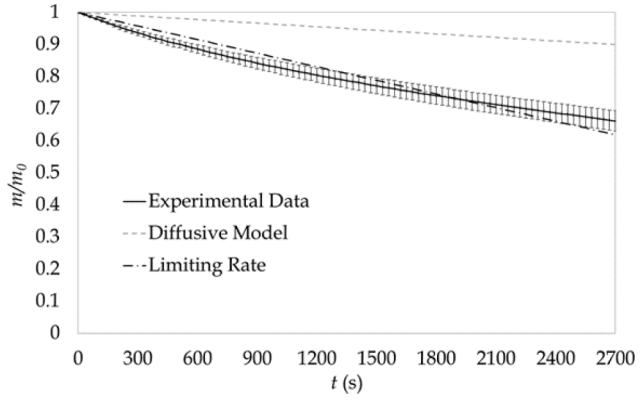

Fig. 17. Mass loss trends for Anode 2 ink (experimental and predicted).

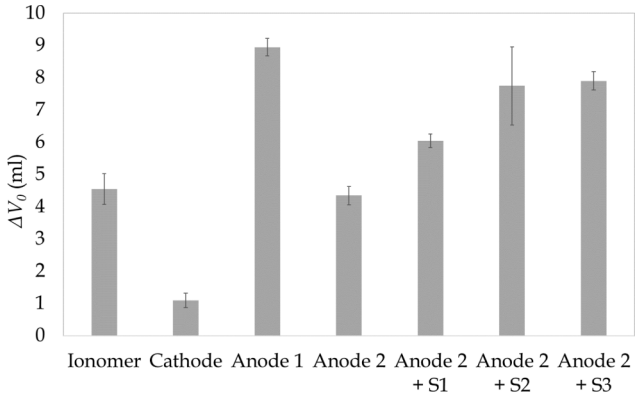

Fig. 18. Foam volume for the tested inks.

far shorter – sometimes instantaneous – lifetime. So, a larger degree of randomness might be justified on physical grounds when some types of surfactants are used; notably, silicone-based surfactants as S2 could yield to a competition between the two described actions, with none of the two certainly prevailing over the other. As for tendency to foam formation, it appears Anode 1 is the most prone, whereas Cathode is the least, which supports the ability of the proposed approach to capture the involved phenomena, since surface tension of water is far lower than that of the alcohol included in the Cathode ink [63], thus making an aqueous ink entrain more air and generate more foam, at least during the air-injection time.

Interestingly, all the surfactants tested as additives to Anode 2 made foam formation increase with respect to the pure ink: in general, it appears that decreasing surface tension implies an increase in bubble volume, regardless of the nature of the employed surfactant. However, testing inks endowed with different surfactant concentrations may lead to different outcomes, especially in the case of non-ionic surfactants; as already mentioned, silicone-based ones may yield an inherent random behavior in terms of foam formation.

In a manner similar to drying kinetics, viscosity may have an effect on foam formation, especially impacting on the force air bubbles have to exert to rise and ultimately leave the liquid surface. However, the here proposed approach is not focused on analyzing that relationship; moreover, no evidence of it arose from the conducted experiments, even because viscosity is rather similar in the tested inks (Fig. 3).

As reported in Sub-section 2.2, the developed approach allows visualizing foam lifetime only when transparent or semi-transparent inks are tested. Fig. 19 shows how foam volume evolves over time for Ionomer, the only transparent ink among those tested. The reported trend (the average over five repeats) between the 20 s and the 45 s mark features a higher uncertainty (up to ±0.3 ml), but in the intervals before and after that one a remarkably lower standard deviation is exhibited. Assessing repeatability of this quantitative evaluation of foam stability is rather complex, since randomness may be mainly associated with statistical lifetime of each individual bubble [65].

The best-fitting value for α coefficient was found equal to 0.024 through an iterative process that minimized RMSE (Root Mean Square Error) between the experimental dataset at the relationship presented in Eq. (17); the procedure included setting volume ratio as air injection stops (i.e., $t = 0$ in Sub-section 2.2) equal to one. The trend predicted by that formulation shows a remarkable agreement with the experimental results, which supports the ability of the developed experimental approach to highlight the exponential decay predicted by the Ross formulation for foam stability [59], reviewed in Sub-section 2.2. Notably, the Ross formulation appears to reproduce the experimental trend qualitatively and falls within the standard-deviation range over a substantial portion of the sampling time.

4. Conclusions

In the present work, an experimental approach consisting of two different setups and procedures was developed to quantitatively evaluate drying kinetics and foam formation in inks typically employed for inkjet printing of PEMFC electrodes and ionomer layers for the membrane. Those experiments are aimed at providing comparison between different inks, thus assessing their printability against issues as nozzle clogging and poor ink release due to foam. Moreover, they support performance assessment of additives commonly employed to address those technical problems. The devised experiments – arguably

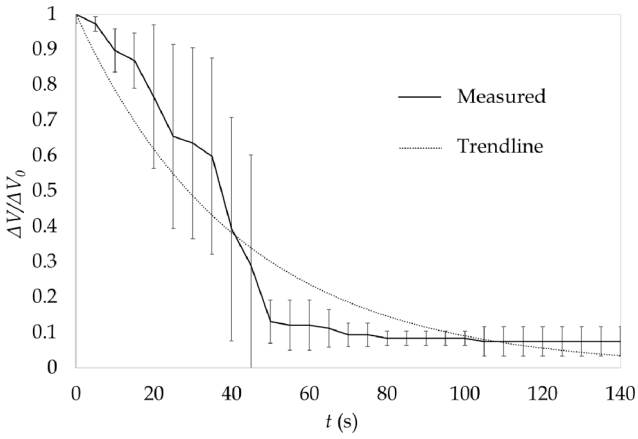

Fig. 19. Foam volume trend for the Ionomer ink: experimental dataset and trend predicted by the Ross formulation [59].

unprecedented as referred to that specific application – are relatively simple and founded on basic concepts: film drying of a suspension or a solution deposited onto a surface in quiescent air; bubble generation by injecting a known air flow rate within a suspension or a solution, which resembles the mechanism occurring in industrial inkjet printers.

As for drying kinetics, the approach appears fully representative of the involved physics, since the inks featuring the most volatile solvents exhibited the higher evaporation rate, calculated on the acquired dataset by approximating differential quantities to finite differences; moreover, experiments with ethylene glycol – well recognized as a humectant that reduces overall evaporation – resulted consistently in lower mass loss trend. Hygroscopicity of pure ethylene glycol was also properly identified. Statistical analysis supports the robustness of the approach, as well as the qualitative results from a predictive formulation based on a classic diffusive model [32,44–47] applied to each of the intervals constituting the sampling time and generated as based on mass-acquisition frequency. A limiting evaporation rate based on the hypothesis of isotropic diffusion was also challenged and applied to the whole evaporation process. Both formulations qualitatively support the experimental findings, yet the quantitative comparison between experimental and predicted datasets reveals some discrepancy that may be related to inks exhibiting anisotropic behavior in terms of diffusion. With regard to foam formation, the developed methodology yielded substantiated evaluation of the tendency displayed by inks in generating bubbles as air is supplied. The capability of producing results consistent with the involved physics is founded on observing that inks with solvents having lower surface tension made the larger volume of foam arise. Moreover, the proposed approach allows assessing performance of surfactants employed as defoamers, even though the inherent randomness related to the dual action of emphasizing bubble generation and reducing bubble lifetime may result in higher experimental uncertainty. The devised methodology is also capable of monitoring foam stability by visualizing bubble volume over time, even though this can be carried out only if the tested inks are transparent or semitransparent (i.e., the ionomer ink, in the present work). Overall qualitative consistency with the exponential decay of foam volume predicted by the Ross formulation [59] appears to strengthen the applicability of the experimental setup to evaluate foam stability, even emphasized by quantitative agreement through most of the sampling time, as the predicted curve falls within the standard-deviation range.

Overall, the proposed approach can be easily implemented in a production environment and yield rapid and robust evaluation of inks towards adapting their formulation to the requirements of inkjet printing, an emerging technique in PEMFC manufacturing.

CRediT authorship contribution statement

Paolo E. Santangelo: Conceptualization, Methodology, Validation, Formal analysis, Investigation, Writing – original draft, Writing – review & editing, Supervision, Project administration. **Marcello Romagnoli:** Conceptualization, Methodology, Formal analysis, Investigation, Resources, Writing – original draft, Supervision, Funding acquisition. **Marco Puglia:** Methodology, Validation, Formal analysis, Investigation, Writing – original draft, Writing – review & editing.

Declaration of Competing Interest

The authors declare that they have no known competing financial interests or personal relationships that could have appeared to influence the work reported in this paper.

Acknowledgments

The authors wish to acknowledge the financial support by FCH JU (Fuel Cells and Hydrogen Joint Undertaking) through the European Union's Horizon 2020 Research and Innovation Action project MAMA-MEA – Mass Manufacture of MEAs Using High Speed Deposition Processes (grant agreement no.: 779591).

References

[1] J. Larminie, A. Dicks, Fuel Cell Systems Explained, Wiley, Hoboken, NJ, USA, 2018.
[2] V. Hacker, S. Mitsushima (Eds.), Fuel Cells and Hydrogen, Elsevier, Amsterdam, The Netherlands, 2018.
[3] N. Guerrero Moreno, M. Cisneros Molina, D. Gervasio, J.F. Pérez Robles, Approaches to polymer electrolyte membrane fuel cells (PEMFCs) and their cost, Renew. Sustain. Energy Rev. 52 (2015) 897–906.
[4] T. Elmer, M. Worall, S. Wu, S.B. Riffat, Fuel cell technology for domestic built environment applications: state of-the-art review, Renew. Sustain. Energy Rev. 42 (2015) 913–931.
[5] X. Lü, Y. Qu, Y. Wang, C. Qin, G. Liu, A comprehensive review on hybrid power system for PEMFC-HEV: issues and strategies, Energy Convers. Manage. 171 (2018) 1273–1291.
[6] F. Barbir, PEM Fuel Cells - Theory and Practice, Elsevier, Amsterdam, The Netherlands, 2012.
[7] B. Millington, S. Du, B.G. Pollet, The effect of materials on proton exchange membrane fuel cell electrode performance, J. Power Sources 196 (2011) 9013–9017.
[8] Y. Hashimasa, Y. Matsuda, M. Akai, Effects of platinum loading on PEFC power generation performance deterioration by carbon monoxide in hydrogen fuel, ECS Trans. 26 (1) (2010) 131–142.
[9] S.-J. Shin, J.-K. Lee, H.-Y. Ha, S.-A. Hong, H.-S. Chun, I.-H. Oh, Effect of the catalytic ink preparation method on the performance of polymer electrolyte membrane fuel cells, J. Power Sources 106 (1-2) (2002) 146–152.
[10] R.R. Passos, V.A. Paganin, E.A. Ticianelli, Studies of the performance of PEM fuel cell cathodes with the catalyst layer directly applied on Nafion membranes, Electrochim. Acta 51 (2006) 5239–5245.
[11] S.J. Peighambardoust, S. Rowshanzamira, M. Amjadi, Review of the proton exchange membranes for fuel cell applications, Int. J. Hydrogen Energy 35 (2010) 9349–9384.
[12] Y. Zheng, Monolithic fuel cell and method, Patent US 6,838,203 B2, 2005.
[13] G.M. Brosseau, Additive manufacturing for fuel cell flow fields, Patent US 9,444,108 B2, 2016.
[14] I. Gibson, D. Rosen, B. Stucker, Additive Manufacturing Technologies: 3D Printing, Rapid Prototyping, and Direct Digital Manufacturing, Springer, New York City, NY, USA, 2015.
[15] M. Cannio, S. Righi, P.E. Santangelo, M. Romagnoli, R. Pedicini, A. Carbone, I. Gatto, Smart catalyst deposition by 3D printing for polymer electrolyte membrane fuel cell manufacturing, Renewable Energy 163 (2021) 414–422.
[16] F.P. Lohmann, P.S.C. Schulze, M. Wagner, O. Naumov, A. Lotnyk, B. Abel, Á. Varga, The next generation solid acid fuel cell electrodes: stable, high performance with minimized catalyst loading, J. Mater. Chem. A 5 (2017) 15021–15025.
[17] B.G. Pollet, A novel method for preparing PEMFC electrodes by the ultrasonic and sonoelectrochemical techniques, Electrochem. Commun. 11 (2009) 1445–1448.
[18] S.A. Mauger, K.C. Neyerlin, A.C. Yang-Neyerlin, K.L. More, M. Ulsh, Gravure coating for Roll-to-Roll manufacturing of Proton-Exchange-Membrane Fuel Cell catalyst layers, J. Electrochem. Soc. 165 (11) (2018) F1012–F1018.
[19] T. Steenberg, H.A. Hjuler, C. Terkelsen, M.T.R. Sánchez, L.N. Cleemann, F.C. Krebs, Roll-to-roll coated PBI membranes for high temperature PEM fuel cells, Energy Environ. Sci. 5 (2012) 6076–6080.
[20] J.W. Ihm, H. Ryu, J.S. Bae, W.K. Choo, D.K. Choi, High performance of electrode with low Pt loading prepared by simplified direct screen printing process in PEM fuel cells, J. Mater. Sci. 39 (2004) 4647–4649.
[21] S. Shukla, K. Domican, K. Karan, S. Bhattacharjee, M. Secanell, Analysis of low platinum loading thin polymer electrolyte fuel cell electrodes prepared by inkjet printing, Electrochim. Acta 156 (2015) 289–300.
[22] F.C. Krebs, Fabrication and processing of polymer solar cells: A review of printing and coating techniques, Sol. Energy Mater. Sol. Cells 93 (4) (2009) 394–412.
[23] S.D. Hoath (Ed.), Fundamentals of Inkjet Printing: The Science of Inkjet and Droplets, Wiley, Hoboken, NJ, USA, 2016.
[24] M. Z. Sengun, Impact of ink evaporation on drop volume and velocity, in: E. Hanson (Ed.), Recent Progress in Ink Jet Technologies II, The Society for Imaging Science and Technology, Springfield, VA, USA, 1999.
[25] M.P. Breton, F.M. Pontes, K.M. Henseleit, B. Helbrecht, M.D. Croucher, R.W. Wong, Ink for ink jet printing, US Patent no. 5,156,675, 1992.
[26] S. Liker, Methods and apparatus for preventing clogging in ink jet printers, patent US5329293A, 1994.
[27] S. Magdassi, Ink requirements and formulations guidelines, in: S. Magdassi (Ed.), The Chemistry of Inkjet Inks, World Scientific, Hackensack, NJ, USA, 2010.
[28] R. Fournier, A.D. Shum, J. Liu, D.C. Sabarirajan, X. Xiao, I.V. Zenyuk, Combined infrared thermography, X-ray radiography, and computed tomography for ink drying studies, ACS Appl. Energy Mater. 1, 6101–6114, 2018.
[29] M. Can, Simultaneous convective heat and mass transfer in impingement ink drying, Int. Commun. Heat Mass Transfer 25 (6) (1998) 863–874.
[30] A. Avci, M. Can, The analysis of the drying process on unsteady forced convection in thin films of ink, Appl. Therm. Eng. 19 (6) (1999) 641–657.
[31] B. Turkan, A.B. Etemoglu, M. Can, An investigation into evaporative ink drying process on forced convective heat and mass transfer under impinging air jets, Heat Mass Transf. 55 (2019) 1359–1369.

[32] H.J. Ward, T.A. Armstrong-Telfer, S.M. Kelly, N.S. Lawrence, J.D. Wadhawan, Evaporative mass loss measurement as a quality control tool for quality assurance in the manufacture of inks suitable for high speed ($\geq$60 m min^{-1}) printing, J. Electroanal. Chem. 872 (2020), 114328.
[33] A.P. Brady, S. Ross, The measurement of foam stability, J. Am. Chem. Soc. 66 (1944) 1348–1356.
[34] A.D. Rudin, Measurement of the foam stability of beers, J. Inst. Brew. 63 (6) (1957) 506–509.
[35] L.G. Phillips, Z. Haque, J.E. Kinsella, A method for the measurement of foam formation and stability, J. Food Sci. 52 (1987) 1074–1077.
[36] L.P.M. Colombo, I.M. Carraretto, A.G. Di Lullo, C. Passucci, A. Allegrucci, Experimental study of aqueous foam generation and transport in a horizontal pipe for deliquification purposes, Exp. Therm Fluid Sci. 98 (2018) 369–380.
[37] P. Amani, S. Hurter, V. Rudolph, M. Firouzi, Comparison of flow dynamics of air-water flows with foam flows in vertical pipes, Exp. Therm Fluid Sci. 119 (2020), 110216.
[38] G. Nishioka, S. Ross, A new method and apparatus for measuring foam stability, J. Colloid Interface Sci. 81 (1) (1981) 1–7.
[39] K. Lunkenheimer, K. Malysa, Simple and generally applicable method of determination and evaluation of foam properties, J. Surfactants Deterg. 6 (1) (2003) 69–74.
[40] C.D. DeBoer, X. Wen, Non-wetting protective layer for ink jet print heads, patent US6345880B1, 2002.
[41] H.W. Coleman, W.G. Steele, Experimentation and Uncertainty Analysis for Engineers, Wiley, New York City, NY, USA, 1999.
[42] F.G. Cottrell, Reststrom bei galvanischer Polarisation, betrachtet als ein Diffusionsproblem, Z. Phys. Chem. 43 (1903) 641–689.
[43] R.P. Buck, T.M. Nahir, R. Mäckel, H.-D. Liess, Unusual, non-Cottrell behavior of ionic transport in thin cells and in films, J. Electrochem. Soc. 139 (1992) 1611.
[44] F.P. Incropera, D.P. DeWitt, T.L. Bergman, A.S. Lavine, Fundamentals of Heat and Mass Transfer, Wiley, Hoboken, NJ, USA, 2006.
[45] N. Perez, Electrochemistry and Corrosion Science, Springer, Boston, MA, USA, 2004.
[46] H.D. Kamaruddin, W.J. Koros, Some observations about the application of Fick's first law for membrane separation of multicomponent mixtures, J. Membr. Sci. 135 (1997) 147–159.
[47] A.F.H. Ward, L. Tordai, Time-dependence of boundary tensions of solutions – I. The role of diffusion in time-effect, J. Chem. Phys. 14 (1946) 453–461.
[48] I. Langmuir, V.J. Schaefer, The effect of dissolved salts on insoluble monolayers, J. Am. Chem. Soc. 59 (1937) 2400–2414.
[49] Y. Saito, A theoretical study on the diffusion current at the stationary electrodes of circular and narrow band types, Rev. Polarogr. 15 (6) (1968) 177–187.
[50] PubChem, Compound summary: Water. Available from: <https://pubchem.ncbi.nlm.nih.gov/compound/Water> (accessed on 13 April 2021).
[51] A. Wexler, Vapor pressure formulation for water in range 0 to 100 °C. A Revision, J. Res. Natl. Bureau Standards – Phys. Chem. 80A (5 and 6) (1976) 775, https://doi.org/10.6028/jres.080A.071.
[52] D. Hendricks, Fundamentals of Water Treatment Unit Processes: Physical, Chemical, and Biological, CRC Press, Boca Raton, FL, USA, 2016.
[53] International Labour Organization (ILO), International Chemical Safety Cards (ICSCs). Available from: https://www.ilo.org/dyn/icsc/showcard.listCards3?p_lang=en (accessed on 7 June 2021).
[54] G.A. Lugg, Diffusion coefficients of some organic and other vapors in air, Anal. Chem. 40 (1968) 1072–1077.
[55] PubChem, Compound summary: 1,2-Ethanediol. Available from: https://pubchem.ncbi.nlm.nih.gov/compound/1_2-Ethanediol (accessed on 13 April 2021).
[56] International Labour Organization (ILO), Ethylene glycol. Available from: <https://www.ilo.org/dyn/icsc/showcard.display?p_version=2&p_card_id=0270> (accessed on 13 April 2021).
[57] P. Fayzi, D. Bastani, M. Lotfi, A note on the synergistic effect of surfactants and nanoparticles on rising bubble hydrodynamics, Chem. Eng. Process. – Process Intensif. 155 (2020), 108068.
[58] A.J. de Vries, Foam stability. Part I. Structure and stability of foams, Recueil des Travaux Chimiques des Pays-Bas, 77, 1958, 81–91.
[59] S. Ross, Bubbles and foams – New general law, Ind. Eng. Chem. 61 (10) (1969) 48–57.
[60] B. Zhmud, F. Tiberg, Surfactants in ink-jet inks, in: D.R. Karsa (Ed.), Surfactants in Polymers, Coatings, Inks and Adhesives, Blackwell, Boca Raton, FL, USA, 2003.
[61] B. Petkova, S. Tcholakova, M. Chenkova, K. Golemanov, N. Denkov, D. Thorley, S. Stoyanov, Foamability of aqueous solutions: role of surfactant type and concentration, Adv. Colloid Interface Sci. 276 (2020), 102084.
[62] P.E. Santangelo, M.A. Corticelli, P. Tartarini, Experimental and numerical analysis of thermal interaction between two droplets in spray cooling of heated surfaces, Heat Transfer Eng. 39 (3) (2018) 217–228.
[63] NIST Chemistry WebBook, SRD 69. Available from: <https://webbook.nist.gov/chemistry/name-ser/> (accessed on 13 April 2021).
[64] D.J. Evans, G.P. Morriss, Transient-time-correlation functions and the rheology of fluids, Phys. Rev. A 38 (1988) 4142–4148.
[65] S.T. Tobin, A.J. Meagher, B. Bulfin, M. Möbius, S. Hutzler, A public study of the lifetime distribution of soap films, Am. J. Phys. 79 (2011) 819.